the present observations. The fact that no symmetrical three-electron-bond species are detected for the meso form can also not be explained by a possible wrong symmetry of the expected SOMO with respect to geometry of the parent molecule. In fact the *Ci* point symmetry fits excellently to a hypothetical symmetric antibonding orbital. This is confirmed by the quantum chemical calculations that predict stable geometries for both the racemic and meso form.

Apparently, the addition process of an extra electron to the diphosphine disulfides is able to discriminate between the several possible radical conigurations in a highly selective way. It is conceivable that the differentiation in the formation of the various electronic and geometric radical configurations is a consequence of the kinetics of the electron-capture process, rather than the result of (small) differences in total energy between the final radical products. In general electron-capture will lead to detectable electron-gain centers provided there is a relatively fast relaxation of the electron acceptor.[19] The relaxation may take the form of bond stretching or bending, or bond breaking, and it should lead to sufficiently deep traps to give detectable radical species. A possible explanation for the formation of a symmetric species in the racemate and asymmetric structures in the meso form can be obtained by assuming that the extra electron reacts with the parent molecules from a direction perpendicular to the plane of the phosphorus and sulfur nuclei. The electron will then first encounter one methyl and one phenyl group for the meso molecules and two methyl or two phenyl groups for the enantiomers *R,R* and *S,S*. Discrimination between a symmetric and an asymmetric radical product can then be rationalized by a difference in the rate of molecular relaxation (e.g., bond bending) in the solid state between the small methyl group and the large phenyl substituent. For the meso form the electron adds preferentially to the side of the methyl group rather than to the side with the phenyl substituent, resulting in an asymmetric radical configuration. For the molecules of the racemate (*R,R* and *S,S*), there is no difference between the relaxation rate of the two sides of the molecule and hence a symmetric electron-capture product is formed.

In the light of the present results further experimental and theoretical study on stereochemical selection in radical formation will be necessary.

Acknowledgment. This investigation has been supported by the Netherlands Foundation of Chemical Research (SON) with financial aid from the Netherlands Organization for the Advancement of Pure Research (ZWO). We thank G. C. Groenenboom for assistance in the quantum chemical calculations.

Registry No. 1, 13639-75-3; **1a**, 115181-91-4; **1b**, 115093-24-8; **2**, 13639-76-4; **2a**, 115181-92-5.

(19) Symons, M. C. R. *Pure Appl. Chem.* **1981**, *53*, 223.

Resonance Raman Studies of Dioxygen Adducts of Cobalt-Substituted Heme Proteins and Model Compounds. Vibrationally Coupled Dioxygen and the Issues of Multiple Structures and Distal Side Hydrogen Bonding

Alan Bruha and James R. Kincaid*

Contribution from the Chemistry Department, Marquette University, Milwaukee, Wisconsin 53233. *Received September 23, 1987*

Abstract: The resonance Raman (RR) spectra of the oxygen adducts of cobalt-substituted heme proteins have been carefully studied in the oxygen–oxygen stretching region. Included in the study are the cobalt analogues of myoglobin (Mb_{Co}), hemoglobin (Hb_{Co}), and its isolated subunits (α_{Co} and β_{Co}) as well as the iron/cobalt mixed hemoglobin hybrids, $(\alpha_{Co}\beta_{Fe})_2$ and $(\alpha_{Fe}\beta_{Co})_2$. The spectra of the $^{16}O_2$, $^{18}O_2$, and scrambled oxygen ($^{16}O_2$:^{16}O–^{18}O:$^{18}O_2$, 1:2:1) adducts have been measured in both normal (H_2O) and deuteriated (D_2O) buffers for each of the proteins. Strong bands located at ~1135, ~1098, and ~1065 cm^{-1} in H_2O solution are identified with $\nu(^{16}O–^{16}O)$, $\nu(^{16}O–^{18}O)$, and $\nu(^{18}O–^{18}O)$, respectively. Shifts of these bands in D_2O solution and the selective appearance of weaker features in the spectra of particular isotopic oxygen adducts are interpreted as the consequence of vibrational coupling of ν(O–O) with internal modes of the proximal and/or the distal histidylimidazole. The plausibility of this interpretation is supported by the observation of similar behavior in model compound systems which is documented here and in earlier studies. All of the major and minor features observed in the spectra of the proteins can be explained without requiring the existence of two liganded (O_2) conformers, in contrast to earlier interpretations. In addition, based on the results of model compound studies, the frequency observed for ν(O–O) indicates that the bound dioxygen is hydrogen bonded to the distal histidylimidazole in these protein systems. However, the present interpretation argues that the frequency shifts of $\nu(^{16}O–^{16}O)$ observed upon replacement of H_2O by D_2O cannot be taken as evidence for this distal side hydrogen bonding. Finally, it is suggested that the spectroscopic consequences of such coupling not only complicate the interpretation of oxygen adduct spectra but also (in a positive light) may provide a powerful spectroscopic probe of subtle structural perturbations once they are more fully understood and properly calibrated.

The oxygen transport proteins, hemoglobin (Hb) and myoglobin (Mb), are perhaps the most thoroughly studied of all biomolecules.[1] Despite intensive effort by many research groups and an extensive body of accumulated knowledge, questions remain unanswered, even at a rather fundamental level. In fact, knowledge of the details of O_2 structure and bonding at the heme site remains incomplete. Thus, issues such as the importance of distal side hydrogen bonding between the bound O_2 and the heme pocket distal histidine[2-7] and even the number of stable structures[7-9] remain controversial.

(1) *Hemoglobins*; Antonini, E., Rossi-Bernardi, L., Chiancone, E., Eds.; Academic Press: New York, 1981; Vol. 76.

(2) Mims, M. P.; Porras, A. G.; Olsen, J. S.; Noble, R. W.; Peterson, J. A. *J. Biol. Chem.* **1983**, *258*, 14219.
(3) Pauling, L. *Nature (London)* **1964**, *203*, 182.
(4) Phillips, S. E. V.; Schoenborn, B. P. *Nature (London)* **1981**, *292*, 81.
(5) Shaanan, B. *Nature (London)* **1982**, *296*, 683.
(6) Shaanan, B. *J. Mol. Biol.* **1983**, *171*, 31.
(7) Phillips, S. E. V. *J. Mol. Biol.* **1980**, *142*, 531.
(8) Potter, W. T.; Tucker, M. P.; Houtchens, R. A.; Caughey, W. S. *Biochemistry* **1987**, *26*, 4699.

0002-7863/88/1510-6006$01.50/0

Vibrational spectroscopy, using both infrared (IR)[10] and resonance Raman (RR)[11-15] techniques, is potentially one of the most effective methods to investigate these issues in that, theoretically, it may serve as a direct probe of vibrational modes associated with the Fe–O_2 linkage; i.e., ν(Fe–O) and ν(O–O). In principle then, insight into the nature and control of O_2 binding can be gained by comparison of directly monitored vibrational behavior of protein-bound O_2 with that observed for well-designed and carefully controlled model compound systems.[16-18] Unfortunately, unambiguous interpretation of the existing data has been prevented by the existence of artifacts and other complications which arise as a result of experimental difficulties[8] and the recently noted propensity for bound O_2 to vibrationally couple with internal modes of the associated molecular framework so as to generate complex vibrational patterns.[8,17,18]

In conducting IR studies, it is possible, in principle, to extract the weak ν(O–O) absorptions from the other bands in this complicated spectral region by employing difference techniques.[10] However, as was discussed in detail by Caughey and co-workers[8] in their recent report of carefully conducted IR studies, many factors can give rise to artifacts in these difference spectra. Moreover, as our parallel RR experiments reported herein confirm, even in the case of these (most thorough) IR studies of oxygenated Hb's and Mb's, extreme complexity in the vibrational behavior of bound O_2 was indicated and ambiguities remained.[8]

Since the first RR spectra of heme proteins were reported by Strekas and Spiro,[19] the technique has been applied by many workers to investigate heme structure in a large number of derivatives.[11-15] Unfortunately, with respect to the issue of interest here, it has not been possible to identify conditions under which the ν(O–O) of oxygenated Hb or Mb is effectively enhanced, thus eliminating the possibility of directly probing the Fe–O_2 fragment by observation of this mode. This obstacle was overcome, in effect, by the work of N. T. Yu and co-workers who demonstrated that the ν(O–O) of the cobaltous analogues is strongly enhanced (presumably via charge-transfer transitions) with excitation at 406.7 nm.[9,13,16] The fact that the cobalt analogues retain the gross structural features and functional properties of the native systems[1,20] validates the utility of RR studies of these as an effective strategy to probe the steric, electronic, and environmental factors which influence oxygen binding.

While the effective enhancement (and thus strong intensities) of ν(O–O) of the cobalt analogues offers certain obvious advantages over corresponding IR studies of weak overlapped bands, the observation of complex vibrational patterns also plagued the RR studies. Thus, Yu and co-workers attributed the appearance of multiple isotope ($^{16}O_2$, $^{18}O_2$) sensitive bands to two distinct structural isomers, suggesting that the $\nu(^{16}O–^{16}O)$ of one of these was vibrationally coupled to a porphyrin core deformation mode.[9,13,16]

Despite this complexity, the potential utility of RR studies of these O_2 adducts is attractive, and other workers have investigated the important issue of hydrogen bond formation involving the distal histidylimidazole, NH.[21] Specifically, comparative studies were carried out in normal (H_2O) and deuteriated buffers. Shifts (in ^2H_2O) of $\nu(^{16}O–^{16}O)$ of +2 to +5 cm^{-1} were observed for oxygen adducts of cobalt analogues of Mb, Hb, and the cobalt-containing subunits of iron/cobalt hybrid hemoglobins. Interestingly, in the recent IR study of oxygenated Hb's and Mb's the IR bands attributed to ν(O–O) were reported to shift by an insignificant amount in ^2H_2O buffers.[8] As will be discussed later, our work confirms the earlier RR results.

Recently, we reported results of RR studies of dioxygen adducts of a series of cobalt porphyrin derivatives in an attempt to define the spectroscopic behavior of ν(O–O) in response to controlled perturbations in steric, electronic, and environmental factors.[17,18] The essential conclusion of that work, from the standpoint of the issue of interest here, was that oxygen–oxygen stretching frequencies of these adducts are not only sensitive to the chemical factors listed above but also exhibit a propensity to vibrationally couple with internal modes of the axial ligand and, perhaps more surprisingly, with modes of an associated solvent molecule (CH_2Cl_2 or toluene). In those works, we showed that strategic isotopic labeling experiments are useful in distinguishing chemically induced frequency shifts from those due to the influence of vibrational coupling effects. In view of these previous studies, we have undertaken a systematic investigation of the behavior of ν(O–O) of O_2 adducts for the cobalt analogues of Mb, Hb, α_{Co},β_{Co}, and Co/Fe hemoglobin hybrids and an appropriate model compound in an attempt to clarify the issues introduced above.

Experimental Section

Protoporphyrin IX (free acid) was purchased from Midcentury Chemical Co. (Posen, IL), HPLC grade heptane, chloroform, 2-butanone, ethyl acetate, isoctane, ^2H_2O (99.8% ^2H), $C^2H_2Cl_2$ (99.6% ^2H), and CH_3O^2H (99.5% ^2H) from Aldrich Chemical Company, and glacial acetic acid from DuPont Chemical Company. All were used without further purification. Methanol was distilled from Mg metal, pyridine from KOH, and CH_2Cl_2 from CaH_2. Lyophilized sperm whale myoglobin, dithiothreitol, (C-100) catalase, and *p*-hydroxymercuribenzoate were obtained from Sigma Chemical Co. The gases, $^{16}O_2$ (Amerigas, 99+%) and $^{18}O_2$ (99%, Monsanto), were used as received.

Model Compound Preparation. [$^2H_1$]4-Methylimidazole (N-deuteriated) was prepared by stirring 50 mg of sublimed 4-methylimidazole (4-MI) in 2.5 mL of CH_3O^2H for 1 h. The CH_3O^2H is removed by vacuum. This process is repeated for a total of three exchanges. The 4-MI-$^2H_1$ is purified by sublimation, and N-deuteriation is confirmed by NMR via the disappearance of the 13.5 ppm (N–H) resonance (TMS standard). Other peaks are not affected. 4-MI was deuteriated at the ring carbon positions by heating 500 mg of 4-MI in 12.5 mL of 1 N NaO^2H at 80 °C for 10 h.[22] This step is repeated once. [$^2H_1$]4-Methylimidazole reaction solution is brought to neutral pH with 5 N ^2HCl and dried on a rotavap. The 4-MI-d_3 is extracted with methanol. The N-deuteriated analogue is reexchanged to 4-MI-d_2 by dissolving in methanol and evaporating to dryness several times. The final product is purified by sublimation. Proton NMR ($C^2H_2Cl_2$ or C^2HCl_3) shows H-2 and H-5 to be greater than 95% deuteriated. The CH_3 and NH peaks exhibit integrated intensity of 3:1, demonstrating that these positions are not deuteriated.

The $^2H_8$ analogue of tetraphenylporphine ([$^2H_8$]TPP) and its cobalt complex were prepared as previously described by using benzaldehyde and [$^2H_5$]pyrrole as starting materials.[18,23,24]

Protein Preparation. Cobalt protoporphyrin (CoPP) was prepared according to literature precedent by using 200 mg of cobaltous acetate and 100 mg of protoporphyrin (PP).[25] The N_2 purged reaction mixture was checked for the presence of free PP by TLC[26] on Silica Gel IB plates (Baker). The free PP fluoresces under long wavelength ultraviolet illumination (Black-Ray UVL-21). The incorporation is generally complete after 10 min. The reaction mixture is cooled in an ice bath and then added to a separatory funnel containing 500–800 mL of saturated aqueous sodium acetate and 200 mL of 2-butanone. Following separation, the organic layer (containing the CoPP) is washed three times with 150-mL portions of 20% (w/w) aqueous sodium acetate and is then reduced to dryness on a rotating evaporator at 40 °C. The residue is

(9) Tsubaki, M.; Yu, N. T. *Proc. Natl. Acad. Sci. U.S.A.* **1981**, *78*, 3581.
(10) Alben, J. O. *The Porphyrins*; Dolphin, D., Ed.; Academic Press: New York, 1978; Vol. III, p 323.
(11) Asher, S. A., ref 1, p 371.
(12) Spiro, T. G. *Iron Porphyrins, Part II*; Lever, A. B. P., Gray, H. B., Eds.; Addison-Wesley Publishing Co.: Reading, MA, 1983; Part II, p 89.
(13) Yu, N. T. *Methods Enzymol.* **1986**, *130*, 350.
(14) Kitagawa, T. *Adv. Infrared Raman Spectrosc.* **1986**, *13*, 443.
(15) Rousseau, D. L.; Ondrias, M. R. *Ann. Rev. Biophys. Bioeng.* **1983**, *12*, 357.
(16) Mackin, H. C.; Tsubaki, M.; Yu, N. T. *Biophys. J.* **1983**, *41*, 349.
(17) Bajdor, K.; Kincaid, J. R.; Nakamoto, K. *J. Am. Chem. Soc.* **1984**, *106*, 7741.
(18) Kincaid, J. R.; Proniewicz, L. M.; Bajdor, K.; Bruha, A.; Nakamoto, K. *J. Am. Chem. Soc.* **1985**, *107*, 6775.
(19) Strekas, T. C.; Spiro, T. G. *Biochem. Biophys. Acta* **1972**, *263*, 830.
(20) Yonetani, T.; Yamamoto, H.; Iizuka, T. *J. Biol. Chem.* **1974**, *249*, 2168.
(21) Kitagawa, T.; Ondrias, M. R.; Rousseau, D. L.; Ikeda-Saito, M.; Yonetani, T. *Nature (London)* **1982**, *298*, 869.
(22) Takeuchi, Y.; Yeh, H. J. C.; Kirk, K. L.; Cohen, L. A. *J. Org. Chem.* **1978**, *43*, 3565.
(23) Bak, B.; Christensen, D.; Hansen, L.; Rastrup-Anderson, J. *J. Chem. Phys.* **1956**, *24*, 720.
(24) Barnett, H. G.; Hudson, M. F.; Smith, K. M. *Tetrahedron Lett.* **1973**, *30*, 2887.
(25) Dickinson, L. C. *J. Chem. Ed.* **1976**, *53*, 381.
(26) Dolphin, D.; DiNello, F. *Anal. Biochem.* **1975**, *64*, 444.

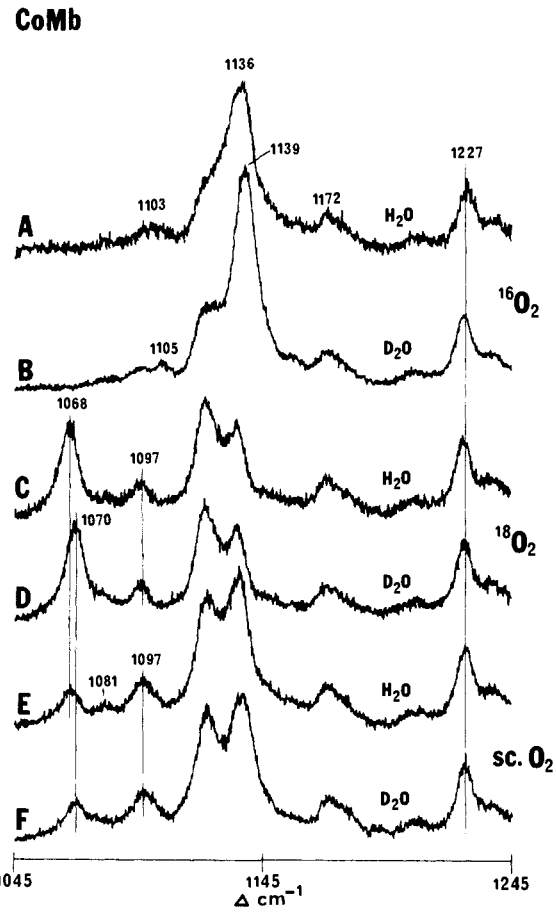

Figure 1. Resonance Raman spectra of cobalt myoglobin at room temperature. 406.7-nm excitation, 5 mW laser power, and 4 cm^{-1} spectral band bass. Solutions are 50 mM Tris·HCl buffer (H_2O or D_2O), pH (pD) 8.3, 50–70 μM in heme, and 1 atm of oxygen.

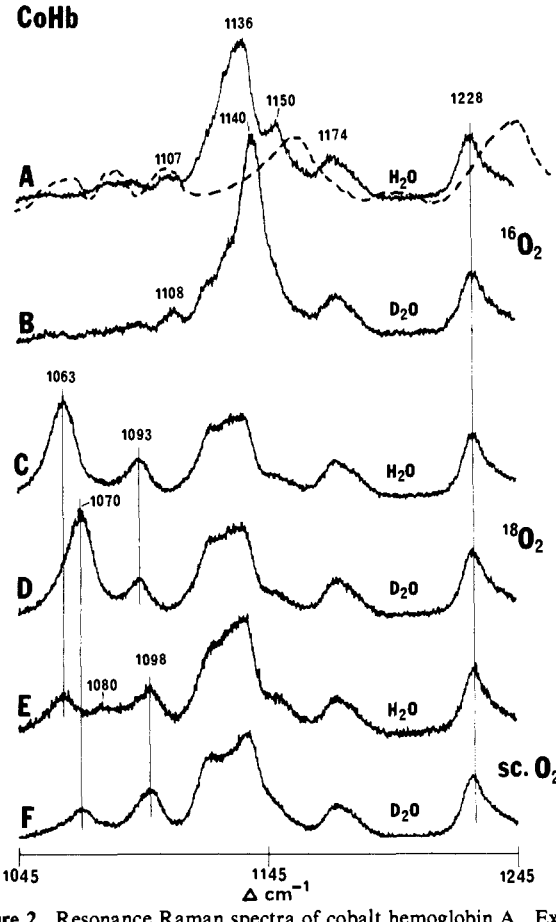

Figure 2. Resonance Raman spectra of cobalt hemoglobin A. Experimental conditions the same as in Figure 1. Dotted line in Figure 2A is L-histidine in H_2O, pH 8.2.

suspended in water, thoroughly washed, and filtered. It is redissolved in methanol and evaporated to dryness to facilitate the removal of bulk water. It is then purified by chromatography as described by other workers.[27] The fraction rich in CoPP is evaporated to dryness, redissolved in ethyl acetate:acetic acid (6:1), and centrifuged to remove insoluble materials. CoPP is recrystallized with 1.5 volumes of *n*-heptane. The crystals were washed twice with *n*-heptane and dried overnight in a vacuum desiccator. The TLC procedure described earlier showed one spot, and the pyridine–NaOH spectrum exhibited peaks at 424, 534, and 568 nm with relative intensities of 180:15.6:16.7 (lit. values (λ_{max} (ϵ mm)) 424 (175), 535 (15.6), and 569 nm (17).[28a]

Hemoglobin (Hb) was isolated from out-dated blood obtained from a local blood center according to established procedures,[29] and apohemoglobin (apo-Hb) was prepared by the acid–butanone method.[30] Reconstitution of apo-Hb with CoPP was carried out according to the published method.[25] The protein samples were exhaustively exchanged in ^2H_2O buffers by concentrating 1 mL of CoHb to 0.05 mL at the centrifuge by using Centricon Microconcentration membranes (C-10 membrane). One mL of 0.05 M Tris-HCl (D_2O) buffer, pH 8.3, was added, and the sample again was concentrated to 0.05 mL. This procedure was repeated three times.

Sperm whale myoglobin was purified according to Yu and co-workers.[9] Heme extraction, CoPP reconstitution, and buffer exchange were carried out as described for hemoglobin. The Fe/Co hybrids were prepared according to the method described by Yonetani.[28b]

Spectral Measurements. Electronic absorption spectra were obtained with a Perkin-Elmer Model 320 spectrophotometer by using 1-mm and 10-mm optical cells. Raman spectra were obtained with a Spex 1403 monochromator equipped with DM1B controller and data station with multiple scan capability. Excitation at 406.7 nm was accomplished with a Spectra-Physics Model 164-01 Kr ion laser. Plasma lines of the excitation source were removed with an Applied Photophysics Model 2300 prism monochromator. Power at the sample was 5–10 mW, and a spectral band pass of 4 cm^{-1} was employed for most measurements. Estimated accuracy is ± 1 cm^{-1}.

Sample preparation and acquisition of low-temperature RR spectra of the cobalt porphyrin complexes was performed as described previously.[17,18] For the protein samples, approximately 0.5 mL of CoHb or CoMb (50–70 μM in cobalt porphyrin) was added to a glass spinning cell, and the spectra were obtained at room temperature. The samples were deoxygenated by purging with nitrogen, and then oxygen ($^{16}O_2$ or $^{18}O_2$) was introduced to a pressure of 1 atm. Scrambled oxygen, $^{16}O_2$:$^{16}O^{18}O$:$^{18}O_2$ (1:2:1), was made by exposing equimolar amounts of $^{16}O_2$ and $^{18}O_2$ to the discharge from a Tesla coil. Molecular seives are included in the bulb used for making scrambled oxygen to aid in the decomposition of ozone. The final isotopic ratios were directly determined by Raman spectroscopy.

Results and Discussion

A. Protein Systems. In Figures 1–6 are shown the RR spectra of the various cobalt-substituted heme proteins which were studied: namely, Mb_{Co}, Hb_{Co}, and the isolated α_{Co} and β_{Co} subunits as well as the Fe/Co hemoglobin hybrids, $(\alpha_{Fe}\beta_{Co})_2$ and $(\alpha_{Co}\beta_{Fe})_2$. The spectra include the region wherein the $\nu(^{16}O-^{16}O)$ and $\nu(^{18}O-^{18}O)$ are expected to occur,[13] i.e., 1100–1150 cm^{-1} for $\nu(^{16}O-^{16}O)$ and 1050–1100 cm^{-1} for $\nu(^{18}O-^{18}O)$. In each figure (corresponding to an individual protein), spectra are given for the $^{16}O_2$, $^{18}O_2$, and "scrambled oxygen" ($^{16}O_2$, $^{16}O-^{18}O$, $^{18}O_2$, 1:2:1) adducts. In addition, for each isotopic oxygen adduct, spectra were obtained in buffered D_2O as well as normal (H_2O) buffers. The porphyrin core deformation modes[12] located at 1228 and 1174 cm^{-1} serve as practically useful approximate internal frequency and intensity standards.

In agreement with Yu and co-workers,[9,13] we observe a number of features in the spectra of the $^{16}O_2$ adducts of Mb_{Co} (Figure 1A) and Hb_{Co} (Figure 2A) which disappear, substantially change

(27) Yonetani, T.; Yamamoto, H.; Woodrow, G., III *J. Biol. Chem.* **1974**, *249*, 682.
(28) (a) Reference 1, p 92. (b) Reference 1, p 117.
(29) Kilmartin, J. V.; Hewitt, J. A.; Wooton, J. F. *J. Mol. Biol.* **1975**, *93*, 1203.
(30) Teale, F. W. *J. Biochem. Biophys. Acta* **1959**, *35*, 543.

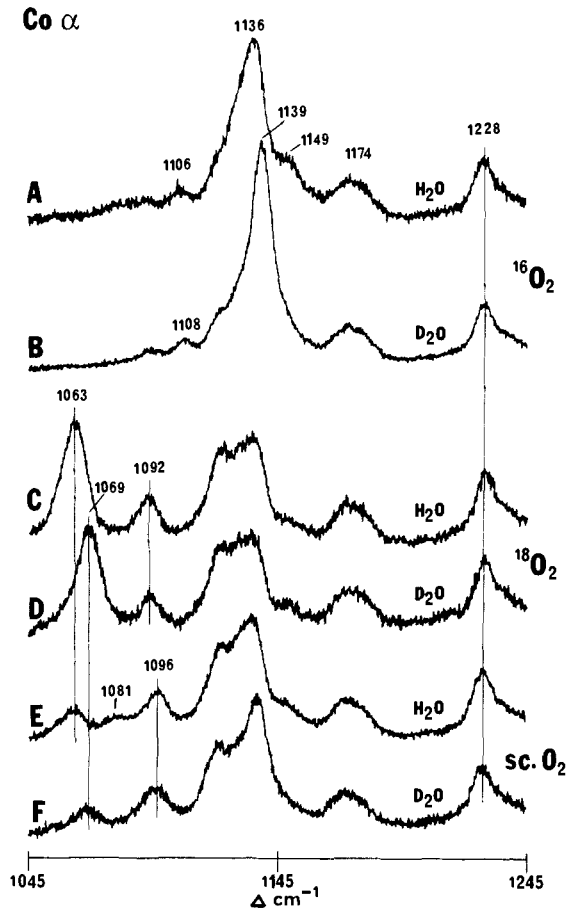

Figure 3. Resonance Raman spectra of cobalt α chains. Experimental conditions the same as in Figure 1.

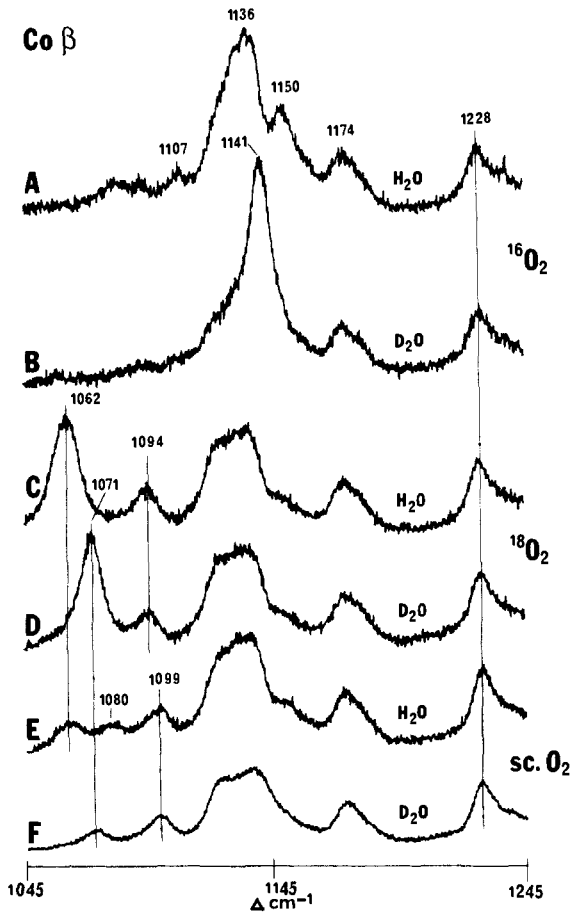

Figure 4. Resonance Raman spectra of cobalt β chains. Experimental conditions the same as in Figure 1.

shape, or undergo intensity changes upon substitution of $^{18}O_2$ (the spectra labeled C in Figures 1 and 2). Thus, comparing the spectra of $^{16}O_2$–Mb_{Co} (Figure 1A) and $^{18}O_2$–Mb_{Co} (Figure 1C), a strong band centered at 1136 cm^{-1} is altered upon $^{18}O_2$ substitution to reveal two resolved bands at 1123 and 1136 cm^{-1}. Also a weak 1103-cm^{-1} band in the $^{16}O_2$ spectrum (Figure 1A) disappears and is replaced by a feature located at 1097 cm^{-1} in the $^{18}O_2$ spectrum. The strongest band in the $^{18}O_2$ spectrum is observed at 1068 cm^{-1} (Figure 1C). The corresponding spectra of the $^{16}O_2$–Hb_{Co} and $^{18}O_2$–Hb_{Co} are even more complex owing to the appearance of the obvious feature located at 1150 cm^{-1} (Figure 2A) in the $^{16}O_2$ spectrum.

The previous interpretation of this complex spectroscopic behavior invoked the existence of two conformers.[9,13] The higher energy conformer was associated with the bands observed at ~1150 cm^{-1} [$\nu(^{16}O–^{16}O)$] and 1095 cm^{-1} [$\nu(^{18}O–^{18}O)$]. The lower energy conformer, wherein the bound O_2 is presumably hydrogen bonded to distal histidylimidazole, was associated with several oxygen isotope sensitive bands. Thus, the relatively strong features observed at 1063 cm^{-1} (CoHb) and 1068 cm^{-1} (CoMb) were assigned to $\nu(^{18}O–^{18}O)$. However, the $\nu(^{16}O–^{16}O)$ of this conformer was considered to be coupled with a nearly coincident porphyrin internal mode occurring at ~1123 cm^{-1}, giving rise to two bands at ~1105 and ~1135 cm^{-1}.

As is discussed in detail below, we have considered an alternative explanation of these spectral patterns which invokes vibrational coupling of the bound dioxygen with internal modes of the proximal, and possibly the distal, histidylimidazole fragments. The presence of such coupling is also expected to lead to spectral changes in D_2O buffers inasmuch as the vibrational frequencies of these fragments are subject to alteration via NH/ND exchange in D_2O. Thus, a clearer understanding of the influence of such coupling on the measured D_2O shifts and on the general vibrational patterns of O_2 adducts in these protein systems requires a detailed analysis of the subtle features observed in all isotopic analogues.

The Origin of Multiple Oxygen Sensitive Bands. The analysis of the $\nu(^{16}O–^{16}O)$ region is complicated by the presence of porphyrin core and substituent modes which may overlap the $\nu(^{16}O–^{16}O)$ mode(s). These are apparent in the spectra of the deoxy derivatives (not shown) and in the spectra of the $^{18}O_2$ analogues (spectra labeled C and D in each of the figures). The positions and intensities of these features vary slightly among the different proteins, but in all cases two bands are observed (sometimes unresolved) at ~1135 and ~1120 cm^{-1}, the latter being at a slightly lower frequency in Mb_{Co} than in Hb_{Co}. These two features have been assigned to a porphyrin core deformation mode (ν_5) and a vinyl mode, respectively.[31] As can be seen by comparison of spectra C and D in each of the figures, as expected, these modes are not affected by D_2O exchange.

The most obvious difference in this spectral region among the various proteins studied is the appearance of a rather prominent mode at 1150 cm^{-1} in the spectra of some of the derivatives, i.e., Hb_{Co}, β_{Co}, and the β subunit of $(\alpha_{Fe}\beta_{Co})_2$ (spectrum A in Figures 2, 4, and 6). In other derivatives this feature is apparently missing or very weak, i.e., Mb_{Co}, α_{Co}, and the α subunit of $(\alpha_{Co}\beta_{Fe})_2$ (spectrum A in Figures 1, 3, and 5). As can also be seen by comparison of spectra A and B in Figures 2 through 6, this band disappears, or is substantially weaker, in D_2O solution. The residual intensity at 1150 cm^{-1} in the $^{18}O_2$ spectra can be reasonably attributed to trace $^{16}O_2$. In addition to the 1150 cm^{-1} feature, a strong band located at ~1135 cm^{-1} is observed in the spectra of the $^{16}O_2$ adducts of all proteins studied. This strong feature is overlapped with the porphyrin macrocycle mode located in this region and appears to upshift by 2–5 cm^{-1} in D_2O buffers.

In the $\nu(^{18}O–^{18}O)$ region, the $^{18}O_2$ adducts of all systems studied exhibit a strong band at ~1063–1068 cm^{-1} which upshifts (2–9 cm^{-1}) in D_2O buffer. On the other hand, the spectra of the

(31) Choi, S.; Spiro, T. G.; Langry, K. C.; Smith, K. M.; Budd, D. L.; LaMar, G. N. *J. Am. Chem. Soc.* **1982**, *104*, 4345.

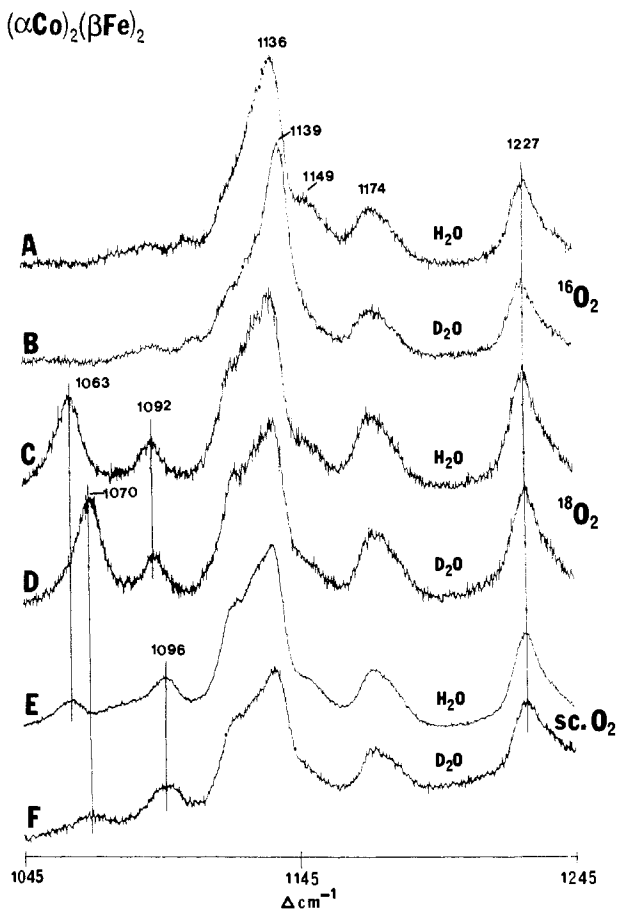

Figure 5. Resonance Raman spectra of $\alpha(Co)_2\beta(Fe)_2$ hybrid hemoglobins. Experimental conditions the same as in Figure 1.

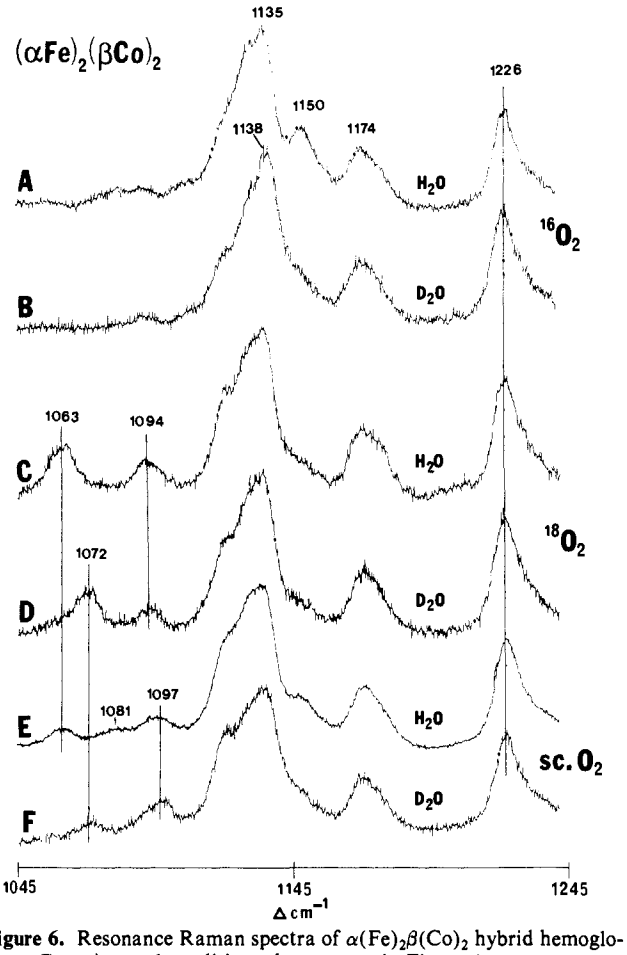

Figure 6. Resonance Raman spectra of $\alpha(Fe)_2\beta(Co)_2$ hybrid hemoglobins. Experimental conditions the same as in Figure 1.

scrambled oxygen adducts of all of the proteins studied exhibit a band at $\sim$1098 cm^{-1} which is apparently not affected by H_2O/D_2O exchange (spectra E and F in Figures 1–6). Thus, in all cases, the strongest O_2 associated bands are observed at $\sim$1135 cm^{-1} [$\nu(^{16}O-^{16}O)$], $\sim$1098 cm^{-1} [$\nu(^{16}O-^{18}O)$], and $\sim$1063[$\nu(^{18}O-^{18}O)$]. The strong $\nu(^{16}O-^{16}O)$ and $\nu(^{18}O-^{18}O)$ are D_2O sensitive, while the $\nu(^{16}O-^{18}O)$ located at 1098 cm^{-1} exhibits no D_2O sensitivity.

In addition to these major bands, a weak (but reproducible) D_2O insensitive band appears at $\sim$1105 cm^{-1} in the spectra of the $^{16}O_2$ adducts of all proteins studied (spectra A and B of all figures). On the other hand, this feature disappears and is replaced by a somewhat stronger feature at $\sim$1095 cm^{-1} in the spectra of the $^{18}O_2$ adducts of all systems. This 1095-cm^{-1} band apparently is not D_2O sensitive (spectra C and D of all figures). Finally, the only other weak feature observed appears at 1080 cm^{-1} in the spectra of the scrambled oxygen adducts of all of the proteins studied (spectra labeled E in each figure). However, in contrast to the two weak features mentioned above (i.e., 1105 and 1095 cm^{-1}), this band disappears in D_2O solution (spectrum F in each figure). Although this feature is particularly weak, its presence in H_2O (and absence in D_2O) for all six proteins is reproducible.

In summary of this section, for certain proteins (Hb_{Co}, β_{Co}, and $(\alpha_{Fe}\beta_{Co})_2$) a rather prominent band is observed at 1150 cm^{-1} in the $\nu(^{16}O-^{16}O)$ region which disappears in D_2O, while the strong $\nu(^{16}O-^{16}O)$ at $\sim$1135 cm^{-1} simultaneously upshifts by 3–5 cm^{-1}. The strong, relatively isolated $\nu(^{18}O-^{18}O)$ exhibits upshifts in D_2O of 2–9 cm^{-1} for all proteins studied, while the $\nu(^{16}O-^{18}O)$ remains D_2O insensitive for all of the proteins. Weak features appear either in the $\nu(^{16}O-^{16}O)$ region (i.e., 1105 cm^{-1}) for the $^{16}O_2$ adduct or in the $\nu(^{18}O-^{18}O)$ region (i.e., 1095 cm^{-1}) for the $^{18}O_2$ adduct. Comparison of the $^{16}O_2$ and $^{18}O_2$ spectra for several of these systems reveals that $^{16}O_2/^{18}O_2$ isotopic shift (calculated from the strongest features at 1135 and 1063 cm^{-1}) may vary considerably from the expected[17,18] 64–66 cm^{-1}.

Behavior such as that described above is similar to that observed in our earlier studies of O_2 adducts of cobalt porphyrin complexes with several pyridine and imidazole axial bases.[17,18] There too, certain of the model systems studied exhibited $^{16}O_2/^{18}O_2$ shifts which were larger (or smaller) than the predicted 64–66 cm^{-1}. However, in the cases studied, deuteriation of the axial ligand resulted in $\Delta\nu(^{16}O_2/^{18}O_2)$ shifts which were 64–66 cm^{-1} (vide infra). In addition, a number of the O_2 adducts (e.g., the pyridine and 1,2-dimethylimidazole (1,2-DMI) complexes) exhibited prominent or weak bands with one oxygen isotope which were absent in the case of the second oxygen isotopomer.

Prompted by these earlier observations, we are inclined to interpret the results for the protein systems in a manner similar to that for the model compounds.[17,18] That is, we suggest that the 1150 cm^{-1} feature in the $\nu(^{16}O-^{16}O)$ region can be attributed to an internal mode of the proximal (or possibly the distal) histidylimidazole fragment which gains intensity as a consequence of vibrational coupling with the nearby $\nu(^{16}O-^{16}O)$ at $\sim$1135 cm^{-1} and that this coupling is decreased upon deuteriation of the imidazole fragment (in D_2O) giving rise both to a decreased intensity (or disappearance) of the 1150-cm^{-1} feature and to a simultaneous upshift in the $\nu(^{16}O-^{16}O)$ at $\sim$1135 cm^{-1}. In addition, the frequency shifts observed for $\nu(^{18}O-^{18}O)$ in D_2O solution indicate that the bound $^{18}O_2$ is vibrationally coupled to a second internal imidazole mode in the 1050–1100 cm^{-1} region. To the extent that such coupling is present, the weak features at $\sim$1105 cm^{-1} ($^{16}O_2$), $\sim$1095 ($^{18}O_2$); and 1080 cm^{-1} (scrambled oxygen) can also be attributed to coupled internal imidazole modes. This suggestion is also consistent with previously reported Raman spectra of aqueous solutions of histidine, which (in the nonprotonated form at pH 8.2) exhibit a broad band at $\sim$1150 cm^{-1} and weaker bands at 1101, 1087, and 1063 cm^{-1}.[32] We have reproduced the reported spectrum and have included it in Figure 2A (dotted line) for comparison with the spectrum of the Hb_{Co} adduct with $^{16}O_2$. The fact that the D_2O sensitive[32] feature at $\sim$1160 cm^{-1} in the histidine

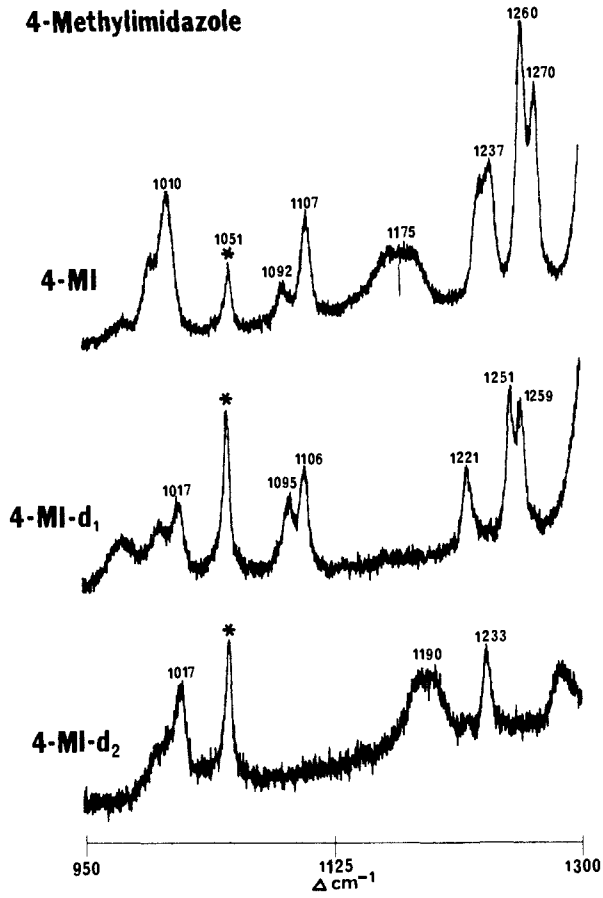

Figure 7. Raman spectra of 4-methylimidazole and deuteriated analogues in $C^2H_2Cl_2$, room temperature, 406.7-nm excitation, and 10 mW laser power. Asterisks mark solvent bands.

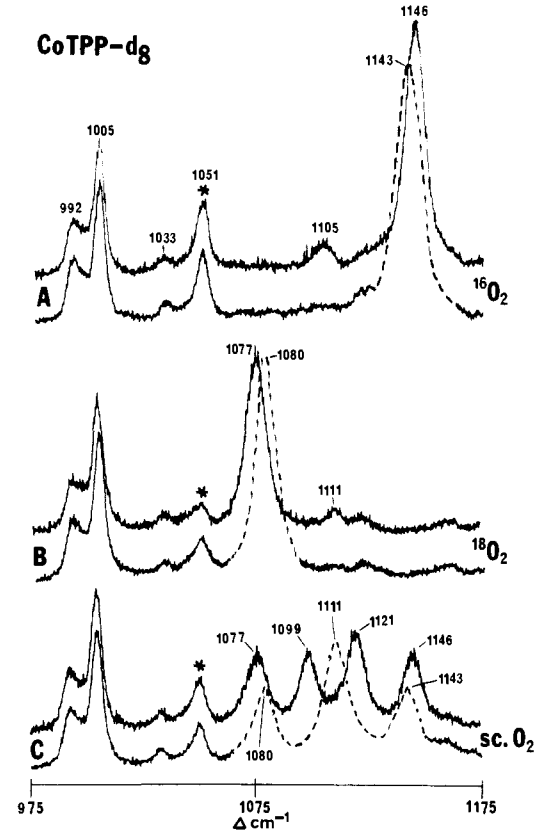

Figure 8. Resonance Raman spectra of CoTPP-d_8 at approximately −90 °C with $C^2H_2Cl_2$, 406.7-nm excitation, 10 mW laser power, and 4 cm^{-1} spectral band pass. (a) Spectra with $^{16}O_2$: solid line, 4-MI; dashed line, 4-MI-d_2; (b) Spectra with $^{18}O_2$: solid line, 4-MI; dashed line, 4-MI-d_2; (c) Spectra with $^{16}O_2$–$^{16}O^{18}O$–$^{18}O_2$ (1:2:1): solid line, 4-MI; dashed line, 4-MI-d_2. Asterisks mark solvent bands.

spectrum is broader than in the Hb_{Co} spectrum is attributed to the difference in environment (aqueous versus heme pocket).

B. Model Compound Studies. The essential point of the above discussion is that the complex spectroscopic behavior exhibited by the protein systems may result from vibrational coupling of the ν(O–O) with histidylimidazole internal modes. In an attempt to demonstrate the plausibility of the above interpretation we have carried out an investigation of a model compound system which incorporates a histidine-like axial ligand. Specifically, we have studied the RR spectra of isotopic oxygen adducts of cobalt tetraphenylporphine (CoTPP) complexes employing 4-methylimidazole (4-MI) and its deuteriated analogues as axial ligands. In order to avoid an annoying overlap of the $\nu(^{18}O–^{18}O)$ with a rather strong 1084 cm^{-1} mode of CoTPP, we have utilized the β-pyrrole deuteriated analogue, Co(TPP-d_8).

The spectra of 4-MI and its N-deuteriated (4-MI-d_1) and ring deuteriated (4-MI-d_2) analogues are given in Figure 7. Several bands are observed in the spectrum of 4-MI (Figure 7A) between 1050 and 1200 cm^{-1} which disappear in the spectrum of 4-MI-d_2 (Figure 7C). While the feature at ~1150 cm^{-1} disappears upon N-deuteriation, two bands remain in this region (1106 and 1095 cm^{-1}, Figure 7B).

The spectra of the dioxygen adducts of the model complex are given in Figure 8. Note that the bands located at ~1122 (i.e., the weak feature in Figure 8, parts A and B), 1033, 1005, and 992 cm^{-1} are porphyrin macrocycle modes while that at 1051 cm^{-1} is due to the solvent, $C^2H_2Cl_2$. This solvent was used to avoid interaction of $\nu(^{16}O–^{16}O)$ with the 1155-cm^{-1} mode of CH_2Cl_2.[17] In the case of the $^{16}O_2$ adduct (Figure 8A—solid line), a strong band attributable to $\nu(^{16}O–^{16}O)$ is observed at 1146 cm^{-1} along with a weak feature at 1105 cm^{-1}. Upon replacing the 4-MI with 4-MI-d_2 (Figure 8A—dotted line), the 1105-cm^{-1} band disappears, and the $\nu(^{16}O–^{16}O)$ simultaneously *downshifts* by 3 cm^{-1}. In the case of the $^{18}O_2$ adduct with 4-MI (Figure 8B—solid line), a strong $\nu(^{18}O–^{18}O)$ is observed at 1077 cm^{-1}. However, in this case the weak feature near 1100 cm^{-1} is observed at 1111 cm^{-1}. Upon replacement of 4-MI with 4-MI-d_2 (Figure 8B —dotted line), the 1111-cm^{-1} band disappears while the $\nu(^{18}O-^{18}O)$ *upshifts* by ~3 cm^{-1}.

Such behavior is entirely consistent with that expected for vibrationally coupled dioxygen. The $\nu(^{16}O–^{16}O)$, having an inherent frequency of 1143 cm^{-1}, interacts with the 1107-cm^{-1} 4-MI mode giving rise to two bands located at 1105 and 1146 cm^{-1} (i.e., the lower frequency component shifts down by 2–3 cm^{-1}, while the higher frequency component upshifts by the same amount). Upon substituting 4-MI-d_2, this coupling is eliminated causing the disappearance of the 1105-cm^{-1} feature and revealing the inherent frequency of $\nu(^{16}O–^{16}O)$ as 1143 cm^{-1}. The $\nu(^{18}O–^{18}O)$, having an inherent frequency of 1080 cm^{-1}, interacts with the 1107-cm^{-1} 4-MI mode to yield two bands which are shifted by ±2–4 cm^{-1} from their inherent frequencies. In this case, the 4-MI band is the higher frequency component and thus experiences an upshift.

These rather subtle manifestations of vibrationally coupled dioxygen are the result of weak coupling between modes which are relatively widely separated (1143–1107 = 36 cm^{-1}). Such effects are more clearly illustrated in the spectra of the scrambled oxygen adducts, Figure 8C. Given inherent $\nu(^{16}O–^{16}O)$ and $\nu(^{18}O–^{18}O)$ frequencies of 1143 and 1080 cm^{-1}, $\nu(^{16}O–^{18}O)$ is predicted to occur at ~1111 cm^{-1}, i.e., midway between 1143 and 1080 cm^{-1}. As can be seen in the case of 4-MI-d_2 (no base mode is present in this region), expected behavior is observed (Figure 8C—dotted line). Thus, three bands are observed having an intensity ratio of ~1:2:1. However, the spectrum observed for the 4-MI complex (Figure 8C—solid line) provides a dramatic illustration of the remarkable spectroscopic effects which can be manifested in the case of strong vibrational coupling (i.e., as the

(32) Ashikawa, I.; Itoh, K. *Biopolymers* **1979**, *18*, 1859.

interacting modes become frequency matched). Thus, the close matching of $\nu(^{16}O-^{18}O)$ (having an inherent frequency of 1111 cm^{-1}) to the interacting base mode at ~1107 cm^{-1} results in efficient coupling which gives rise to two strong bands located at ±8–10 cm^{-1} from their inherent frequencies of ~1107 and 1111 cm^{-1} (i.e., at 1099 and 1121 cm^{-1}). As we have recently shown, precisely analogous behavior has been observed in the case of the scrambled oxygen adduct of the 3,5-dichloropyridine complexes with cobalt porphyrins.[33]

We have carried out similar studies by using the N-deuteriated analogue, 4-MI-d_1, with the result that no frequency shifts or intensity changes are observed. Such behavior is consistent with expectations based on the lack of a significant shift of the interacting 1107-cm^{-1} mode upon N-deuteriation (Figure 7B). Thus, inasmuch as this axial ligand internal mode is not affected by N-deuteriation, the coupling strengths are not affected, and the ν(O–O) frequencies of the various oxygen isotopomers are identical with those of the 4-MI analogues.

We wish to point out that we note a weak interaction of $\nu(^{18}O-^{18}O)$ with the solvent, $C^2H_2Cl_2$. Thus, the inherent frequency of $\nu(^{18}O-^{18}O)$ is actually 1078 cm^{-1}. This is determined by obtaining spectra of the 4-MI-d_2 complex in CH_2Cl_2. When $C^2H_2Cl_2$ is the solvent, the $\nu(^{18}O-^{18}O)$ interacts with the 1051-cm^{-1} solvent mode and is upshifted to ~1080 cm^{-1}. This minor complication obviously does not invalidate the conclusions reached regarding the axial ligand mode interaction.

C. Comparison of Model Compounds and Protein Systems. Several spectroscopic features are clearly demonstrated in the model compound study described above. First, the major spectral bands, attributable to ν(O–O), can be observed to shift upon deuteriation of the axial ligand. In this case the shift is entirely attributable to vibrational coupling effects (deuteriation at the 2 and 5 positions of 4-MI is a chemically inocuous substitution). Such behavior mimics the observed upshifts of the 1063- and 1135-cm^{-1} bands in the protein systems upon N–H/N–D exchange of the histidylimidazole. In addition, the experiments with scrambled oxygen illustrate the point that "new bands" may appear in the spectrum of one isotopic oxygen adduct that are not observed in the spectra of other oxygen isotopomers. In the present model compound work, a new band appears at 1099 cm^{-1} in the spectrum of the scrambled oxygen adduct. Also, in our previous work we had shown that an internal pyridine mode is observed at 1067 cm^{-1} in the spectrum of the $^{18}O_2$ adduct of the Co(TPP-d_8)–pyridine complex (close to the $\nu(^{18}O-^{18}O)$ at 1082 cm^{-1}) and that this 1067-cm^{-1} feature is not observed in the corresponding $^{16}O_2$ adduct.[17] Such behavior in the protein systems would provide an explanation for the selective appearance of the 1105 ($^{16}O_2$), 1095 ($^{18}O_2$), and 1080 cm^{-1} ($^{16}O-^{18}O$) features.

While the present and previous[17,18,33] model compound studies document the general spectroscopic manifestations of vibrationally coupled dioxygen, the spectroscopic behavior observed for the proteins is not precisely duplicated by the model system used here. The most obvious difference is the lack of shifts in the model system upon NH/ND exchange. Thus, in order to induce shifts in ν(O–O) in the model system it was necessary to employ ring deuteriated 4-MI. Also, a D_2O sensitive band is clearly observed in certain of the proteins which apparently corresponds to the broad ~1150 cm^{-1}, D_2O sensitive, band observed in the spectrum of histidine (Figure 2A, dotted line). A similar band is observed in the spectrum of 4-MI at 1175 cm^{-1} (Figure 7A), but it is not enhanced in the model compound system (Figure 8). In the model systems, all oxygen isotopomers are clearly coupled to a single internal 4-MI mode which occurs at 1107 cm^{-1} in the spectrum of free 4-MI, while in the protein systems the $\nu(^{16}O-^{16}O)$, $\nu(^{18}O-^{18}O)$, and $\nu(^{16}O-^{18}O)$ appear to be coupled to several modes.

The failure to precisely mimic the spectroscopic behavior of the protein systems does not seriously weaken the argument for vibrationally coupled dioxygen in the proteins since several structural features of the protein active site, which may be important in dictating the nature of the vibrational coupling, are not readily modeled. For example, in the protein active site both the proximal and distal histidylimidazole fragments are positioned to couple with bound dioxygen. Although several planned time-resolved RR studies may distinguish proximal versus distal coupling, model compound studies are required to investigate the effects of each. The present study and one of our previous[17] studies convincingly demonstrated coupling with the trans-axial ligand. While another of our previous studies[18] documented coupling with an intimately associated solvent molecule, a more sophisticated model (perhaps containing an appended imidazole positioned to hydrogen bond with the bound O_2) will be required to properly investigate coupling effects with the distal histidylimidazole.

It is also difficult to adequately model the vibrational characteristics of the proximal histidylimidazole. Thus, while 4-MI may be a *chemically* reliable model, its vibrational modes may be sufficiently different from those of coordinated histidylimidazole so as to exhibit different coupling behavior (i.e., the steric and electronic factors which control coupling of O_2 with particular internal ligand modes are not well-defined). This is a difficult issue to address in that what are needed are the vibrational frequencies of heme coordinated 4-MI and histidylimidazole rather than those of the free ligands. This is necessary because 4-MI (as well as histidylimidazole) coordinates to the iron as the sterically favored 5-MI tautomer.[4,34,35] This is an important consideration inasmuch as Ashikawa and Itoh have shown that there are relatively large (>40 cm^{-1}) frequency differences (for some bands) in the spectra of these tautomers.[32]

Another factor which may be important in determining the nature of the coupling with the proximal histidine is the relative orientation of the imidazole plane and the plane defined by the Co–O–O fragment. In the proteins, the relative orientation of these fragments is controlled by hydrogen bonding of the bound dioxygen to the distal histidine (vide infra) and by tertiary constraints on the proximal imidazole. In the model systems such control is not readily achieved.

We had noted in previous work[17] that ligand internal modes near 1150 cm^{-1} are enhanced in the cases of 2-methylimidazole (2-MI) and 1,2-dimethylimidazole (1,2-DMI). However, the ~1175-cm^{-1} mode of 4-MI (free ligand spectrum, Figure 7A) is not similarly enhanced in the present study. The apparent differences in the spectroscopic behavior of dioxygen adducts involving these two chemically and structurally similar ligands (4-MI and 2-MI) are not readily explainable. We do note that the dihedral angle which the ligand plane assumes with respect to the plane defined by the porphyrin N–Co–N axis is expected to be different for the 2-MI (and 1,2-DMI) compared to 4-MI. According to Scheidt and Chipman,[34] 4-MI (coordinated 5-MI) is expected to assume a nearly eclipsed orientation, while 2-MI (and other sterically hindered ligands) is expected to assume larger values (i.e., a so-called staggered orientation).

While the importance of this factor is difficult to assess without properly designed model systems, we do note an interesting correlation of spectroscopic behavior with this structural parameter in the proteins studied. The available crystal structure data for oxy-Mb[7] and oxy-Hb[6] give the values of the plane orientation angles as 1° for oxy-Mb, 11° for the α subunit, and 27° for the β subunit of oxy-Hb. The relative intensities of the ~1150-cm^{-1} feature in the protein spectra (spectrum A of each figure) vary in the same order. Thus, the more staggered β subunit (27°) exhibits a more prominent 1150-cm^{-1} feature than does the α subunit (11°) while this feature is virtually absent for oxy-Mb (1°).

In summary of this section, present and previous[17,18] model compound studies document vibrational coupling of bound O_2 to internal modes of the trans-axial ligand and dramatically illustrate potentially remarkable spectroscopic consequences (e.g., Figure 8C). However, it is especially difficult to reliably model the

(33) Proniewicz, L. M.; Nakamoto, K.; Kincaid, J. R. *J. Am. Chem. Soc.*, in press.

(34) Scheidt, W. R.; Chipman, D. M. *J. Am. Chem. Soc.* **1986**, *108*, 1163.

(35) Scheidt, W. R.; Lee, Y. J. *Structure and Bonding*; Buchler, J. W., Ed.; Springer-Verlag: Berlin, 1987; Vol. 64, p 1.

interactions which may exist in the protein systems inasmuch as it is necessary not only to duplicate the relevant steric arrangements but also to closely match the internal modes of two fragments which may potentially interact with the bound O_2 (i.e., the proximal and distal histidylimidazoles). While the absence of such sophisticated models prevents duplication of the steric, electronic, *and vibrational* characteristics present in the protein active site, the proposed coupling scheme provides a reasonable alternative interpretation of the observed complex spectroscopic behavior and has important implications for two fundamental issues, namely, the possible existence of two liganded structures and the presence of hydrogen bonding of the bound O_2 to the distal histidylimidazole.

D. The Issue of Multiple-Liganded Structures. The observation of multiple oxygen-sensitive bands in the RR spectrum of Hb_{Co} and Mb_{Co} has been interpreted previously as evidence for the existence of two structural conformers,[9] in agreement with a reported crystal structure for oxy-Mb.[7] Also, during the preparation of the manuscript, an IR study of oxygenated Mb's and Hb's appeared which also ascribed the appearance of multiple oxygen sensitive bands to the presence of two liganded structures.[8] While the present interpretation does not exclude the possibility of two conformers (e.g., both may exhibit comparable oxygen stretching frequencies), it does not require the existence of a second conformer.

The previous interpretation of the protein spectra assigned the $\sim$1150-cm^{-1} feature to $\nu(^{16}O-^{16}O)$ of a non-hydrogen bonded conformer and the 1095-cm^{-1} band ($^{18}O_2$ adduct) to the corresponding $\nu(^{18}O-^{18}O)$. The second conformer (apparently the major form, based on the intensities of ν(O–O)) was associated with the 1063-cm^{-1} band [$\nu(^{18}O-^{18}O)$] and the *two bands* which are observed at $\sim$1105 cm^{-1} (weak) and $\sim$1135 cm^{-1} (strong); i.e., the $\nu(^{16}O-^{16}O)$ was considered to be coupled with an internal mode of the porphyrin core at $\sim$1125 cm^{-1} to yield the two observed bands. However, the subsequent and present H_2O/D_2O experiments[21] led us to question this interpretation. Thus, the $\sim$1150-cm^{-1} band disappears in D_2O, but the 1095-cm^{-1} band is unaffected. If these corresponded to a single high frequency conformer, a D_2O effect would likely be manifested in both. It can also be noted (in our spectra and in those given in previous works) that the relative intensities of these two bands vary in the spectra of different proteins. Thus, while the 1150-cm^{-1} feature is missing or extremely weak in the spectrum of Mb_{Co} (Figure 1A) and relatively strong in the spectrum of Hb_{Co} (Figure 2A), the intensities of the 1095-cm^{-1} feature (relative to the strong feature near 1065 cm^{-1}) are comparable in Figures 1C and 2C.

The second (major) conformer was associated with the bands at $\sim$1125 cm^{-1} (unperturbed $\nu(^{16}O-^{16}O)$ value) and 1063 cm^{-1}. Thus, these sets of assignments for the two proposed conformers would imply that the ν(O–O) is $\sim$30 cm^{-1} lower for the major (hydrogen bonded) conformer than for the more weakly bound [higher ν(O–O)] minor conformer. Given the results of model compound studies,[16-18] it is difficult to rationalize such a large frequency difference for two such closely related structures.[7]

Our first study[17] provided evidence that hydrogen bonding of the bound O_2 with alcohol additives can lead to 3–5-cm^{-1} shifts to lower frequency. While the relative orientation of the O_2 and distal histidyl-NH in the heme pocket may lead to stronger hydrogen bonding, it does not seem reasonable to attribute a 30-cm^{-1} shift to hydrogen bond formation. Our second study[18] demonstrated a linear correlation of ν(O–O) with the pK_a of the trans-axial ligand for a series of pyridine derivatives. However, the ν(O–O) varied by only $\sim$15 cm^{-1} as the K_a of the pyridine derivative varied by 9 orders of magnitude. Thus, it does not seem reasonable to invoke pK_a changes in the proximal imidazole (the origin of which would not be obvious) to account for this difference. While arguments can be made[8] that the orientation of the imidazole plane (with respect to the plane formed by the Fe–O–O fragment) might substantially affect the frequency of ν(O–O), it is difficult to obtain supporting evidence. The observed [ν(O–O)] frequencies for the model compound which employed 4-MI and 1,2-DMI are not significantly different; i.e., the $\nu(^{18}O-^{18}O)$ bands are observed at $\sim$1075 and 1079 cm^{-1}, respectively. However, further studies with more sophisticated model compounds will be required to properly evaluate the importance of this effect.

The above arguments suggest that it is unlikely that the subtle structural difference observed in the oxy-Mb structure determination[7] could lead to a 30-cm^{-1} difference in the frequencies of the two conformers. Moreover, such a large shift in ν(O–O) is expected to be accompanied by shifts in ν(Co–O) [or ν(Fe–O) in the native systems].[13] Despite intensive efforts by ourselves and others,[13] no evidence for two ν(Co–O) [or ν(Fe–O)] in Mb_{Co} or Hb_{Co} (or the native systems) has been obtained. In contrast to the earlier description, the present interpretation does not require the existence of two conformers having ν(O–O)'s separated by 30 cm^{-1}.

As a final point in this section, it is important to comment on the appearance of the weak, D_2O sensitive, 1080-cm^{-1} feature in the spectra of the adducts with scrambled oxygen. Given the previous interpretation that the $\nu(^{18}O-^{18}O)$ of the lowest energy (H-bonded) conformer occurs near 1065 cm^{-1}, the corresponding $\nu(^{16}O-^{18}O)$ is not expected to occur below $\sim$1095 cm^{-1}. Thus, the appearance of the 1080-cm^{-1} feature only in the spectrum of the scrambled oxygen adduct lends strong support to the proposed enhancement of histidylimidazole modes. That is, this feature is observed only in those cases in which a strong ν(O–O) occurs in the 1100-cm^{-1} region [i.e., $\nu(^{16}O-^{18}O)$]. Such behavior is directly analogous to the selective appearance of the 1099-cm^{-1} feature in the spectrum of the scrambled oxygen adduct of the model system (Figure 8).

E. Shifts in the Deuteriated Buffers and the Issue of Distal Side Hydrogen Bonding. Hydrogen bond formation between bound dioxygen and the distal histidyl $N_\delta H$ is now generally accepted as a potentially important factor in the control of O_2 binding, yet definitive evidence for the existence of this bond remains scarce.[2] Given the efficient enhancement of ν(O–O) in the cobalt-substituted proteins, earlier workers recognized the potential for investigation of this issue by RR spectroscopy.[21] Reasoning that ν(O–O) of hydrogen-bonded O_2 may be sensitive to deuterium substitution, these workers studied the effect of D_2O exchange on the frequencies of $\nu(^{16}O-^{16}O)$ for the $^{16}O_2$ adducts of Mb_{Co}, Hb_{Co}, and the Hb mixed hybrids, $(\alpha_{Fe}\beta_{Co})_2$ and $(\alpha_{Co}\beta_{Fe})_2$. They reported small upshifts of $\nu(^{16}O-^{16}O)$ in D_2O (+2 cm^{-1} for Mb_{Co} and the α_{Co} subunit of $(\alpha_{Co}\beta_{Fe})_2$, +4 cm^{-1} for the β_{Co} subunit of $(\alpha_{Fe}\beta_{Co})_2$, and +5 cm^{-1} for Hb_{Co}). These shifts were reasonably interpreted to be the result of the change from the hydrogen–oxygen bond to the deuterium–oxygen bond, although the authors were careful to point out that other factors might contribute to these shifts. For example, slight changes in the position of the distal histidine might result from subtle tertiary structural changes in the deuteriated protein.

In the present work, this study has been extended to include corresponding experiments with $^{18}O_2$ and "scrambled oxygen" ($^{16}O_2$:$^{16}O-^{18}O$:$^{18}O_2$, 1:2:1) in order to monitor the effect of D_2O exchange on $\nu(^{18}O-^{18}O)$ and $\nu(^{16}O-^{18}O)$ as well as $\nu(^{16}O-^{16}O)$. As can be seen by comparison of spectra labeled A and B in each of the figures, our results for $\nu(^{16}O-^{16}O)$ are in agreement with the previous RR work[21] (i.e., shifts of +2 to +5 cm^{-1} are observed). However, as can be seen by comparison of spectra C and D in each of the figures, the effect of D_2O exchange on $\nu(^{18}O-^{18}O)$ is quite different in several cases; e.g., α_{Co} exhibits a +6-cm^{-1} shift for $\nu(^{18}O-^{18}O)$ but only +3 cm^{-1} for $\nu(^{16}O-^{16}O)$. In addition, in all of the protein systems studied, the $\nu(^{16}O-^{18}O)$ located at $\sim$1098 cm^{-1} is apparently not affected by D_2O exchange (spectra E and F in each figure).

It seems unlikely that the shifts observed in the spectra of the dioxygen adducts upon H_2O/D_2O exchange are the result of changes in the distal side hydrogen bond strength, irrespective of whether such changes are induced by the inherent difference in the strengths of the hydrogen–oxygen and deuterium–oxygen bonds or by tertiary structural changes which repostion the distal histidine. Interestingly, the wide variation in the behavior of the different isotopic ν(O–O) features apparently rules out any *purely*

structural interpretation of the shifts inasmuch as structural and bonding changes are expected to have similar effects on each of the dioxygen isotopomers of a given protein. In fact, for one of the protein systems studied, the shift for one isotopic ν(O–O) is 9 cm^{-1} different from that for another isotopomer (i.e., $\nu(^{18}O–^{18}O)$ and $\nu(^{16}O–^{18}O)$ of the β subunit, Figure 4).

As is clear from the discussion in previous sections of this work, H_2O/D_2O exchange (which leads to NH/ND exchange of the histidyl imidazole fragments) may differentially alter the vibrational interaction between the various isotopomer ν(O–O)'s and the imidazole modes, thus giving rise to a wide variation in observed H_2O/D_2O shifts. To the extent that such shifts cannot then be ascribed to changes in hydrogen bond strength, they cannot be taken as evidence for distal side hydrogen bonding.

We wish to emphasize that the present interpretation does not imply that distal side hydrogen bonding is nonexistent but simply that the observed H_2O/D_2O shifts are the result of altered vibrational coupling patterns rather than altered hydrogen bond strengths. In fact, the ν(O–O) frequencies observed for the proteins and the model compounds are consistent with the distal side hydrogen bonding proposal. Thus, the proteins exhibit $\nu(^{16}O–^{16}O)$ and $\nu(^{18}O–^{18}O)$ at ~1135 and ~1065 cm^{-1}, respectively. The corresponding values for various (non-hydrogen bonded) models are ~1145 and ~1075 cm^{-1} (Figure 8 and ref 16–18). As our earlier model compound study had shown,[17] shifts of this magnitude (~10 cm^{-1}) may reasonably be ascribed to hydrogen bonding to the distal histidylimidazole.

Conclusions

The general vibrational patterns and appearance of multiple oxygen-sensitive bands in the RR spectra of oxygenated cobalt-substituted heme proteins can be rationalized by the proposal that the bound dioxygen is vibrationally coupled to internal modes of the proximal or distal histidylimidazole. The effects of such coupling can generally be demonstrated with model compound studies, to the extent that reliable models can be devised (i.e., certain subtle structural features of the protein are difficult to duplicate). This interpretation provides plausible explanations for observed D_2O and oxygen isotopomer shifts as well as the appearance of weak secondary bands without requiring the existence of two liganded structures and, in fact, would indicate that if two such conformers do exist in solution, they exhibit similar values of ν(O–O).

Finally, while the apparent vibrational coupling of bound dioxygen with internal modes of histidylimidazole complicates the spectral interpretation, it is interesting to consider the potential utility of such measurements. Thus, rather than representing an experimental nuisance, it offers promise as a spectroscopic probe of internal modes of histidine and its interaction with the heme. For example, if the observed intensity of the feature located at 1150 cm^{-1} is indeed correlated with the proximal histidyl plane-orientation angle as the comparison of the limited data might suggest, it would serve as a relatively convenient probe of this possibly important[34] structural parameter. In addition to studies of static systems, useful experiments involving spectroscopic transients are conceivable. Further documentation of this effect and determination of the factors which lead to effective coupling will require the study of more sophisticated model compounds as well as modified and mutant hemoglobins. Such studies are currently underway in our laboratory, and several time-resolved RR studies to probe spectroscopic transients are planned.

Acknowledgment. We gratefully acknowledge support of this work from the National Institutes of Health (DK 35153) and the National Science Foundation (CHE-8413956).

Registry No. 4-MI, 822-36-6; 4-MI-$^2H_1$, 2519-73-5; 4-MI-d_3, 115482-88-7; 4-MI-d_2, 115482-89-8; PP, 553-12-8; CoPP, 14325-03-2; CH_3O^2H, 1455-13-6; NaO^3H, 14014-06-3; cobaltous acetate, 71-48-7.

Crystal Structure, CP/MAS ^{129}Xe, and ^{13}C NMR of Local Ordering in Dianin's Compound Clathrates†

F. Lee, E. Gabe, J. S. Tse, and J. A. Ripmeester*

Contribution from the Division of Chemistry, National Research Council of Canada, Ottawa, Ontario K1A 0R9, Canada. *Received December 9, 1987*

Abstract: The ^{129}Xe and ^{13}C CP/MAS NMR spectra of xenon-containing clathrates of Dianin's compound (4-*p*-hydroxyphenyl-2,2,4-trimethylchroman) are more complicated than expected for fully ordered materials. Single-crystal X-ray diffraction was used to show that there is a single site for xenon in the structure, the only variable being the site occupancy. The NMR spectra therefore were interpreted in terms of small differences in local order. The NMR spectrum of trapped xenon is sensitive to the absence or presence of a second guest in the double cage and in some instances also is sensitive to the nature of this guest as well as the guests in adjoining cages. There is no evidence for preferential formation of Xe dimers in the cages. NMR spectroscopy allows a description of the clathrate which is largely complementary to the structural data from X-ray diffraction.

In recent years, ^{129}Xe NMR, due to the great sensitivity of the Xe nuclear shielding to the Xe atom's physical surroundings, has become an important tool in the study of a variety of phenomena. These include the study of site occupancies in clathrate hydrates,[1,2] other inclusion compounds,[3] and zeolites[4-8] as well as the probing of solution structure[9-12] including hydrophobic interactions in protein and micellar solutions.

Recently two approaches[13,14] have been suggested to account for ^{129}Xe NMR shifts in zeolites. One approach correlates the ^{129}Xe shift with mean free path,[13] the other with surface curvature.[14] However, neither of these can be used to explain the anisotropic chemical shifts observed in solid-like environments.[3] Once a detailed understanding of ^{129}Xe shielding is obtained there

† NRCC no. 28802.

(1) Ripmeester, J. A.; Davidson, D. W. *Bull. Magn. Reson.* **1980**, *2*, 139.
(2) Davidson, D. W.; Handa, Y. P.; Ripmeester, J. A. *J. Phys. Chem.* **1986**, *90*, 6549.
(3) Ripmeester, J. A. *J. Am. Chem. Soc.* **1982**, *104*, 209.
(4) Ito, T.; Fraissard, J. *Proceedings of the 5th Conference on Zeolites*; Heyden: London, 1981; p 510.
(5) de Menorval, L. D.; Fraissard, J. P. *J. Chem. Soc., Faraday Trans. 1* **1982**, *78*, 403.
(6) Ripmeester, J. A. *J. Magn. Reson.* **1984**, *56*, 247.
(7) Ito, T.; Fraissard, J. *J. Chem. Phys.* **1982**, *76*, 5225.
(8) Ito, T.; de Menorval, L. C.; Guerrirer, E.; Fraissard, J. *Chem. Phys. Lett.* **1984**, *111*, 271.

0002-7863/88/1510-6014$01.50/0 Published 1988 by the American Chemical Society